Ultramicroscopy 148 (2015) 25–30

Contents lists available at ScienceDirect

Ultramicroscopy

journal homepage: www.elsevier.com/locate/ultramic

Three-wave electron vortex lattices for measuring nanofields

C. Dwyer *, C.B. Boothroyd, S.L.Y. Chang, R.E. Dunin-Borkowski

Ernst Ruska-Centre for Microscopy and Spectroscopy with Electrons, Peter Grünberg Institute, Forschungszentrum Jülich, D-52425 Jülich, Germany

ARTICLE INFO

Article history:
Received 17 May 2014
Received in revised form
18 August 2014
Accepted 21 August 2014
Available online 1 September 2014

Keywords:
Vortex
Vortex lattice
Holography
Partial coherence

ABSTRACT

It is demonstrated how an electron-optical arrangement consisting of two electron biprisms can be used to generate three-wave vortex lattices with effective lattice spacings between 0.1 and 1 nm. The presence of vortices in these lattices was verified by using a third biprism to perform direct phase measurements via off-axis electron holography. The use of three-wave lattices for nanoscale electromagnetic field measurements via vortex interferometry is discussed, including the accuracy of vortex position measurements and the interpretation of three-wave vortex lattices in the presence of partial spatial coherence.

1. Introduction

Apart from their intrinsic appeal from a fundamental perspective, vortical electron wavefields may prove very useful for the measurement of nanoscale electromagnetic fields. A number of methods have now been demonstrated for producing vortical electron wavefields, ranging from holographic masks [1] to optical aberrations [2,3]. In addition to isolated vortices, methods for producing both light and electron wavefields containing arrays of vortices have also been pursued. One possible application of electron vortex arrays is to use the vortices as fiducial markers to measure an electromagnetic field via its effect on the phase of the wavefield. Such approaches, often termed "vortex interferometry", have been proposed [4] and applied [5,6] in light optics. Vortex interferometry permits a real-space approach to phase retrieval [6], and compared to most Fourier-space reconstruction schemes, has advantages in that it enables a direct measurement of the unwrapped phase, as well as potentially enabling better spatial resolution by bypassing the requirement of sideband separation.

A light or an electron vortex consists of a point at which the amplitude of the wavefield is zero, and around which the phase of the wavefield winds by some (non-zero) integer multiple of 2π. The number of 2π windings, taking into account the sign of the winding as an anticlockwise path is traversed, determines the topological charge of the vortex. A vortex lattice is a periodic array of such vortices. The phenomenon of vortex lattice generation from the interference of three, or more, coherent, non-coplanar plane waves has been studied extensively [7–11]. In light optics, plane waves possessing the required coherence are usually generated experimentally by amplitude division of laser light in an interferometer [6,8,12,13], though vortex lattice generation by wavefront division has also been analyzed [14] and demonstrated experimentally [15].

In the case of electrons, several methods are available for generating multiple interfering plane waves and hence vortex lattices. Perhaps the most obvious of these is amplitude division via diffraction from a crystal, where vortices can be generated when the diffracted beams interfere in the image plane [16]. However, to be useful for electromagnetic field measurements, the generation and interference of the plane waves must be performed in a highly controllable and repeatable way. This is unlikely to be achieved using the method just stated. On the other hand, it *can* be achieved by wavefront division of the beam using multiple electron biprisms [17,18]. Such an approach has been demonstrated recently, where two orthogonal biprisms were used to generate four-wave interference patterns containing electron vortices [19]. In fact, similar four-wave interference experiments were demonstrated and discussed in detail much earlier [18], though not specifically in relation to vortices.

For four interfering waves, however, the existence of a vortex at a point of zero intensity is dependent on the relative phases of the waves, and for certain relative phases non-vortical intensity zeros are obtained instead [9,19]. Moreover, four-wave vortices can follow rather complicated paths in three-dimensional space, and they can exhibit vortex creation and annihilation [9], meaning that the vortices can be present at some positions along the optic axis, and not others. However, most importantly, four-wave vortices are unstable with respect to a perturbation in the phase of one of the waves, an aspect that was also emphasized in the work of Eastwood

* Corresponding author.
E-mail address: c.dwyer@fz-juelich.de (C. Dwyer).

http://dx.doi.org/10.1016/j.ultramic.2014.08.011
0304-3991/

et al. [6]. Hence, the use of four interfering waves is ill-suited to vortex interferometry.

Three-wave vortex lattices, on the other hand, are considerably simpler, though to the best of the authors' knowledge, this is the first work to consider them for electrons. An intensity zero produced by three interfering plane waves is guaranteed to contain a vortex. Under free-space propagation, three-wave vortices trace out straight parallel lines, and they do not exhibit creation or annihilation [7,9]. They are also stable with respect to a phase perturbation in one of the waves [6]. A three-wave vortex lattice is also robust with respect to coherent lens aberrations, which merely cause a rigid displacement of the lattice. Hence the conditions for three-wave vortices are considerably more relaxed, potentially enabling them to be used more effectively for electromagnetic field measurements via electron vortex interferometry.

The present work demonstrates the generation and phase measurement of three-wave electron vortex lattices using a transmission electron microscope (TEM) equipped with three electron biprisms. Two biprisms are used to create a three-wave lattice. However, as with all vortex lattices, the interference patterns, taken alone, contain an ambiguity: there exist two lattice configurations, of opposite topological charges, that have identical interference patterns [20]. To prove unequivocally the existence of vortices, and to resolve the topological charge ambiguity, a phase measurement scheme is required. In this work, a third biprism is therefore used to perform a phase measurement of the vortex lattice, including the topological charge, by means of off-axis electron holography. It is shown that this approach enables a relatively simple generation and measurement scheme for three-wave electron vortex lattices.

2. Theoretical background

This section briefly reviews the theory of three-wave vortex lattices. Consider the electron wave function resulting from the coherent superposition of three, non-coplanar plane waves, which for the moment are assumed to be of unit amplitude:

$$\psi(x) = e^{2\pi i k_a \cdot x} + e^{2\pi i k_b \cdot x} + e^{2\pi i k_c \cdot x}, \tag{1}$$

where x is a three-dimensional position vector, and k_a, k_b, k_c are the wave vectors. A coordinate system is chosen such that the z axis, the optic axis, is normal to the plane defined by the tips of the vectors k_a, k_b, k_c. In this coordinate system, the three wave vectors have a common z component k_z, and the wave function can be written in the form

$$\psi(\mathbf{x}, z) = e^{2\pi i k_z z}(e^{2\pi i \mathbf{k}_a \cdot \mathbf{x}} + e^{2\pi i \mathbf{k}_b \cdot \mathbf{x}} + e^{2\pi i \mathbf{k}_c \cdot \mathbf{x}}), \tag{2}$$

where bold symbols denote two-dimensional vectors lying transverse to the optic axis. Factoring out one of the plane waves, plane wave C, say, the wave function can be written in the form

$$\psi(\mathbf{x}, z) = e^{2\pi i \mathbf{k}_c \cdot \mathbf{x}} e^{2\pi i k_z z}(1 + e^{2\pi i \mathbf{k}_{ac} \cdot \mathbf{x}} + e^{2\pi i \mathbf{k}_{bc} \cdot \mathbf{x}}), \tag{3}$$

where $\mathbf{k}_{ac} = \mathbf{k}_a - \mathbf{k}_c$ and $\mathbf{k}_{bc} = \mathbf{k}_b - \mathbf{k}_c$.

The existence of a vortex requires that the absolute value of the wave function vanishes at the vortex position (since the phase at that position is undefined). This demands that the three terms contained in the parentheses in Eq. (3) sum to zero. Pictorially, if each of these three terms is drawn as a phasor in the complex plane, the phasors must form a closed triangle. A closed triangle can actually be formed in two distinct ways, giving rise to vortices and antivortices, respectively, as shown schematically in Fig. 1a. Hence vortices and antivortices correspond to the phase conditions

$$\mathbf{k}_{ac} \cdot \mathbf{x}_{mn}^{\pm} = m \pm \tfrac{1}{3}, \quad \mathbf{k}_{bc} \cdot \mathbf{x}_{mn}^{\pm} = n \mp \tfrac{1}{3}, \tag{4}$$

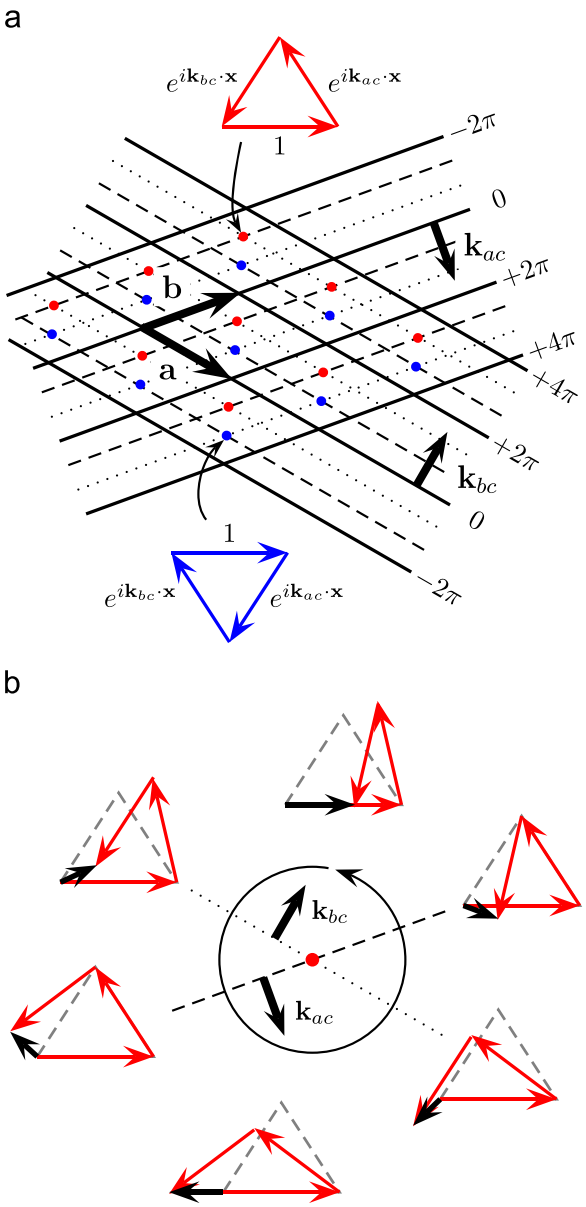

Fig. 1. Schematic representation of a three-wave vortex lattice. (a) The wave function in a plane perpendicular to the optic axis (as defined in the text). Vortices and antivortices (red and blue dots, respectively) exist wherever the three phasors form a closed triangle in the complex plane. The lattice vectors **a** and **b** are the duals of the transverse wave vectors $\mathbf{k}_{ac}$ and $\mathbf{k}_{bc}$, respectively. (b) The evolution of the phasor sum as an anticlockwise path is traversed around a vortex. The phasor sum (black arrow) is seen to acquire a phase of $+2\pi$. (For interpretation of the references to color in this figure caption, the reader is referred to the web version of this paper.)

where m and n are integers, and the upper and lower signs apply to vortices and antivortices, respectively. By defining the vectors **a** and **b** to be the duals of $\mathbf{k}_{ac}$ and $\mathbf{k}_{bc}$, the vortex and antivortex positions are given by $\mathbf{x}_{mn}^{\pm} = (m \pm 1/3)\mathbf{a} + (n \mp 1/3)\mathbf{b}$, where the different values of m and n give rise to a periodic vortex lattice in two dimensions. It is noted the vortex positions are independent of z. Hence, in three-dimensional space each vortex will trace out a line parallel to the optic axis as it was defined above.

The fact that, under the stated conditions, a point of vanishing absolute value *must* contain a vortex (or antivortex) is demonstrated pictorially in Fig. 1b. There we see that the resultant of the three-phasor sum necessarily acquires a phase of $+2\pi$ (or -2π for an antivortex) as an anticlockwise path is traversed in the immediate neighborhood of the point in question. Note that the

factor $e^{2\pi i \mathbf{k}_c \cdot \mathbf{x}}$, which has been factored out in Eq. (3), serves only to modulate the local orientation of the three phasors. This factor can be neglected in the immediate vicinity of a vortex and therefore cannot affect the presence of a vortex. Similarly, the existence of a vortex is uninfluenced by the factor $e^{2\pi i k_z z}$, which serves only to rotate all phasors by the same amount. As the wavefield progresses along the optic axis z, the latter factor gives rise to the well-known helical (antihelical) motions in the immediate vicinities of the vortices (antivortices).

For simplicity, it was assumed above that the three plane waves are of equal amplitude. However, it is easy to imagine that this assumption can be relaxed somewhat, and that a vortex lattice is still obtained provided that the phasors of the three plane waves can form closed triangles in the complex plane. It is also easy to imagine that three-wave vortices are stable against phase perturbations in one (or more) of the plane waves, and that such perturbations will give rise to distortions in the vortex lattice [6]. Moreover, a three-wave vortex lattice is robust against coherent lens aberrations, which, under the isoplanatic approximation, simply offset the relative phases of the waves and cause only a rigid displacement of the lattice.

3. Three-wave vortex lattices

Experiments were performed using a Titan 80–300 FEG-TEM (FEI Co.) operated at 300 kV and in standard conditions with the objective lens switched on. (The experiments in the present work could also be conducted in Lorentz mode, as would be appropriate for magnetic field measurements.) The microscope is equipped with three electron biprisms, though only two biprisms are needed to generate a three-wave vortex lattice. The first biprism (BP1) is located in the illumination system at the plane of the third condenser lens (which was turned off). The second biprism (BP2) is located in an extra lens inserted between the diffraction lens and the imaging aberration corrector, while the third biprism (BP3) is in the selected-area aperture position [21,22]. Normally, when the extra lens is turned on, BP2 is in an image plane while BP3 is just upstream of an image plane.

A three-wave electron vortex lattice can be generated using two biprisms. The optics is adjusted so that the biprisms lie in optically-conjugate planes, and the angle between the two biprisms is set to approximately 60°. This produces, in a plane downstream of the biprisms, regions of two-, three- and four-wave interference as shown schematically in Fig. 2. The regions of three-wave interference can be maximized by suitably defocusing the biprisms. It is noted that if the angle between the biprisms is set to 90°, as done in previous works [18,19], then three-wave regions are not obtained.

Fig. 3 shows an experimental interference pattern produced by BP2 and BP3 with bias settings +333 and +131 V, respectively. This interference pattern was achieved by adjusting the extra lens so that BP2 and BP3 were optically-conjugate, and then adjusting the intermediate and diffraction lenses to optimize the biprism defocus. The interference pattern in Fig. 3 exhibits regions of two-, three- and four-wave interference, with the number of waves being proportional to the average intensity in each region (compare with Fig. 2b). The three-wave regions, which are of interest here, contain an approximately-hexagonal set of fringes with a spacing of about 0.08 nm (relative to the specimen plane). The field of view in the three-wave regions is roughly 10 nm across. Such a fringe spacing and field of view are suitable for vortex-holographic measurements of an electric field at approximately 0.2 nm spatial resolution. In the case of magnetic field measurements, for which Lorentz mode would be required to maintain a magnetic field-free condition at the specimen, the magnification between the specimen and BP2/BP3 would be reduced by a factor of approximately 10, so that the field of view and spatial resolution would increase and decrease by this same factor, respectively.

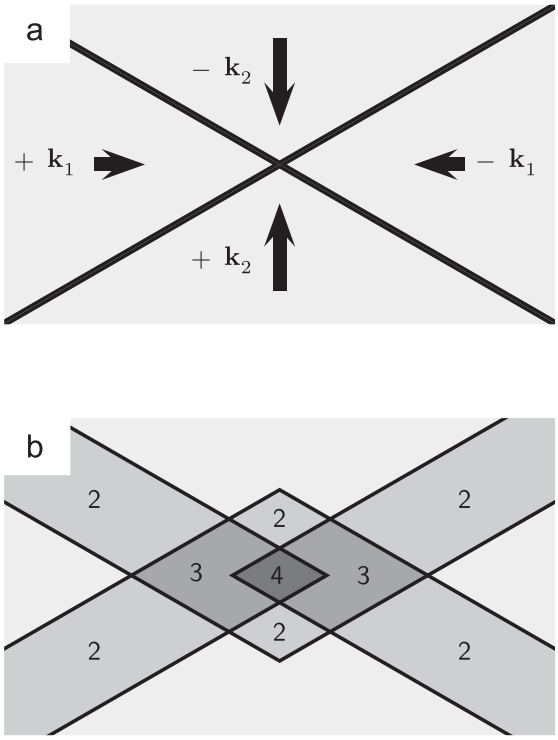

Fig. 2. The effect of two optically-conjugate positively-biased electron biprisms separated by an angle of 60°. (a) The electron wavefield in a plane conjugate to the biprisms experiences transverse momenta indicated by the arrows. (b) After free-space propagation over a finite distance, the wavefield consists of regions of two-, three-, and four-wave interference, which can be rationalized by considering the lateral displacements arising from the momenta indicated in a.

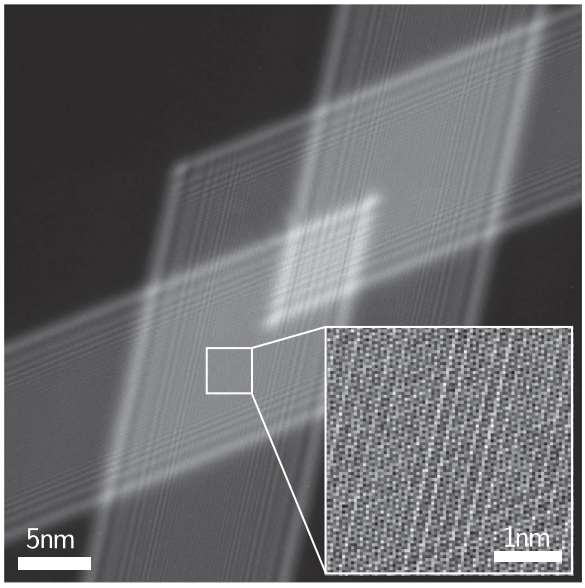

Fig. 3. Interference pattern produced by BP2 and BP3 containing regions of two-, three- and four-wave interference. The three-wave regions contain vortex lattices with a fringe spacing of 0.08 nm and a useable field of view approximately 10 nm wide.

Fig. 4 shows a similar interference pattern, except this time produced by biprisms BP1 and BP2, using bias settings of +156 and +48 V, respectively. In this case, the bias settings were chosen

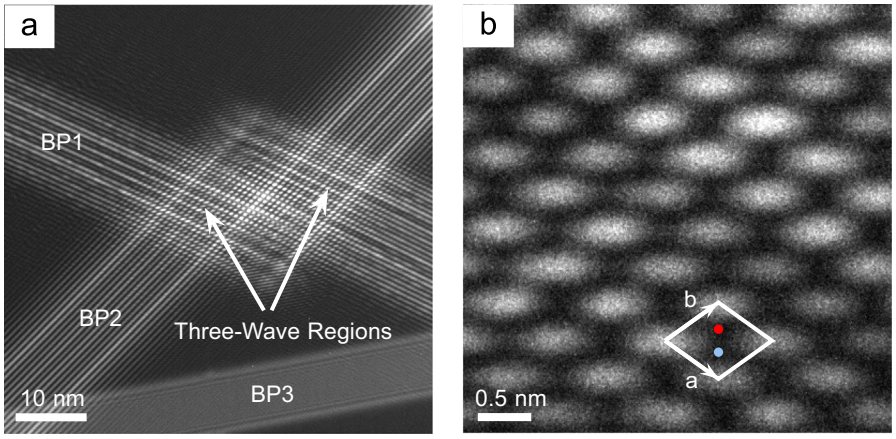

Fig. 4. (a) Interference pattern produced by biprisms BP1 and BP2 containing regions of two-, three-, and four-wave interference (a separate two-wave region caused by BP3 is also visible at the bottom). (b) High-magnification view of one of the three-wave regions exhibiting a fringe spacing of approximately 1 nm (this image has been rotated by 10° with respect to a). The unit cell vectors **a** and **b** are the duals of $\mathbf{k}_1+\mathbf{k}_2$ and $\mathbf{k}_1-\mathbf{k}_2$, where $\mathbf{k}_1$ and $\mathbf{k}_2$ are defined in Fig. 2. The red and blue dots indicate the anticipated positions of vortex and antivortex positions. (For interpretation of the references to color in this figure caption, the reader is referred to the web version of this paper.)

to give approximately 1 nm fringes from both biprisms. This fringe spacing is coarser than that in the previous example, the reason for which will be made clear below. As a point of detail, here the objective lens strength had to be reduced to make the biprisms optically conjugate, and then the extra lens was adjusted to optimize the biprism defocus. The relative positions of the biprisms and the objective lens meant that BP1 was magnified by about three times relative to BP2. Also, the unavoidable higher magnification of BP1 meant that the effect of Fresnel fringes from the edges of this biprism was larger, and that the fringe contrast was lower, due to biprism instabilities, than for BP2.

4. Phase measurement of the vortex lattice

The existence of vortices in the three-wave interference patterns was verified by utilizing the third biprism in the microscope to perform off-axis holography. Hence biprisms BP1 and BP2 were used to generate a three-wave vortex lattice (with the same settings as Fig. 4), while BP3 was used for the holographic phase measurement. The bias of BP3 was set to +80 V.

Fig. 5a shows the interference pattern produced by the three biprisms. BP3 is positioned such that a reference wave is made to interfere with the three-wave regions. Fig. 5b shows a high-magnification view of the interference pattern in a three-wave region, which contains a near-hexagonal set of 1 nm fringes (from BP1 and BP2), and a set of 0.1 nm fringes (from BP3) which are forked at the vortex positions. Close inspection of the forked fringes reveals the position and sign of the vortices: the vortices form an approximately hexagonal lattice with a vortex–antivortex pair in each unit cell. As expected, the vortex positions occur at the intensity minima.

The interference pattern in Fig. 5b was processed using conventional Fourier-holographic methods. During the processing, the sideband's origin was chosen to coincide with one of the three plane waves (that corresponding to $\mathbf{k}_1$ in Fig. 2). Fig. 5c shows a color representation of the retrieved phase, which proves unequivocally the existence of vortex–antivortex pairs forming an approximately-hexagonal lattice.

In the phase measurement described above, the interferences' fringes introduced by BP3 must be fine enough to resolve the vortex lattice. This can be couched in terms of the requirement that the sideband in Fourier space remains well-separated from the centerband, or, alternatively, that the fringes introduced by BP3 are at least three times finer than the vortex lattice. This is a basic requirement regarding the spatial resolution of the Fourier-holographic method. To this end, the bias settings of BP1 and BP2 were deliberately chosen to produce a rather coarse vortex lattice, so that a phase measurement with BP3 was then possible.

5. Vortex position accuracy

In an application of vortex interferometry, the accuracy with which the vortex positions can be measured determines the phase accuracy of the technique. While the holographic phase measurement in Fig. 5 verifies the presence of vortices, it is likely that the vortex positions, as determined from the retrieved phase, are less accurate than those determined from the zeros (or minima) in the three-wave intensity pattern. This occurs because, in Fourier holography, some of the signal tends to be lost due to partial coherence between the object and reference waves, as well as the non-ideal modulation transfer function (MTF) of the CCD camera. Hence, it is more accurate to locate the vortices as intensity minima in a three-wave interference pattern such as Fig. 4b, since partial coherence and MTF effects will be less deleterious.

The intensity $I(\mathbf{x})$ in the vicinity of a vortex (e.g. in Fig. 4b) can be described by a quadratic function in two dimensions, denoted here as $Q(\mathbf{x},\mathbf{p})$ for some set of parameters $\mathbf{p}$. Such a quadratic function can always be written in the form $Q(\mathbf{x})=(\mathbf{x}-\mathbf{x}_0)^T\mathbf{M}(\mathbf{x}-\mathbf{x}_0)+c$, where $\mathbf{M}$ is a real symmetric 2×2 matrix and $\mathbf{x}_0$ is the location of the extremum. Hence locating an intensity minimum (vortex) can be viewed as finding the best-fit parameters $\mathbf{p}=(\mathbf{x}_0,\mathbf{M},c)$. It is assumed that the fit will minimize the reduced chi-squared error $\hat{\chi}^2(\mathbf{p})=N_{DOF}^{-1}\sum_i(I_i-Q_i(\mathbf{p}))^2/\sigma_i^2$, where σ_i^2 is the expected squared error in the intensity at the ith pixel, and N_{DOF} is the number of degrees of freedom. If Poisson statistics can be assumed, then $\sigma_i^2=\langle I_i\rangle\approx I_i$. The squared error in the fitting parameters is given by $\sigma_{\mathbf{p}}^2=\hat{\chi}^2$ diag(cov), where diag(cov) represent the diagonal elements of the parameter covariance matrix [23].

Such an analysis applied to Fig. 4b gave a vortex position accuracy of ≈ 5 pm (sub-pixel accuracy). Given that the spacing of the three-wave lattice is approximately 1 nm, such an accuracy in the vortex positions amounts to a phase resolution of approximately $2\pi/200$. Naturally, the phase resolution obtained depends on the signal-to-noise ratio in the interference pattern, which is itself determined by the illumination conditions and the exposure time. For finer lattices capable of higher spatial resolution, the

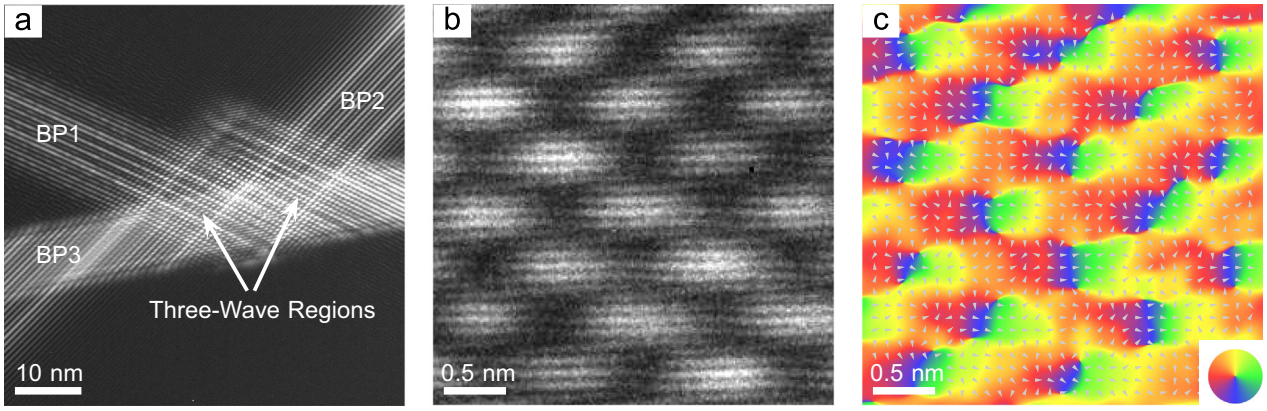

Fig. 5. Holographic phase measurement of three-wave vortex lattice. (a) The interference pattern produced by biprisms BP1, BP2 and BP3. (b) High-magnification view of three-wave region exhibiting forked interference fringes at the vortex positions (this image has been rotated 10° with respect to a). (c) Color representation of the retrieved phase with arrows indicating the direction of the local phase gradient. Vortices correspond to points where the different colors meet, as in the phase color wheel at lower right. Alternatively, vortices and antivortices correspond to points around which the phase gradient winds clockwise or anticlockwise. (For interpretation of the references to color in this figure caption, the reader is referred to the web version of this paper.)

phase resolution will tend to be lower (all other parameters kept constant).

6. Coherence requirements for stable three-wave lattices

In Figs. 3 and 4, the vortices correspond to intensity minima rather than intensity zeros, which results mainly from the finite transverse spatial coherence of the electron beam and the biprism instability. From a theoretical perspective, the partial spatial coherence and instabilities mean that the wavefield cannot be described by a single wave function. Rather, the wavefield must be described as either an incoherent superposition of partial wave functions, a density matrix, or a Wigner distribution. Hence, the interpretation of a vortex lattice actually requires further consideration, since the intensity does not vanish at any point. While there is a significant body of literature devoted to what are termed "coherence vortices" (see [24] and references therein), the special case of three-wave interference allows a particularly simple analysis and interpretation, which is presented below. The reader is forewarned that the considerations below concern the partial coherence of the vortex lattice itself, and not the coherence between the "object" and "reference" waves that is typically considered in off-axis holography.

Partial spatial coherence (as well as instabilities more rapid than the exposure time) can be included by introducing an effective incoherent source distribution $S(\mathbf{x})$. In the ideal case that the source is point-like and located on the optic axis, then $S(\mathbf{x})=\delta(\mathbf{x})$, and the coherent three-wave interference pattern is given by

$$\begin{aligned} I(\mathbf{x}) &= |\psi(\mathbf{x})|^2 \\ &= |e^{2\pi i\mathbf{k}_a\cdot\mathbf{x}}+e^{2\pi i\mathbf{k}_b\cdot\mathbf{x}}+e^{2\pi i\mathbf{k}_c\cdot\mathbf{x}}|^2 \\ &= 3+2\ \cos(2\pi\mathbf{k}_{ab}\cdot\mathbf{x})+2\ \cos(2\pi\mathbf{k}_{bc}\cdot\mathbf{x})+2\ \cos(2\pi\mathbf{k}_{ca}\cdot\mathbf{x}), \end{aligned} \tag{5}$$

where $\mathbf{k}_a$, $\mathbf{k}_b$, $\mathbf{k}_c$ are the transverse wave vectors, and $\mathbf{k}_{ab}$, $\mathbf{k}_{bc}$, $\mathbf{k}_{ca}$ are the differences in these wave vectors. On the other hand, for a centrosymmetric but otherwise arbitrary effective source $S(\mathbf{x})$, the cosine terms (which correspond to interfering plane waves) are weighted in the following manner:

$$\begin{aligned} I(\mathbf{x}) = 3 &+ S_{ab}\ \cos(2\pi\mathbf{k}_{ab}\cdot\mathbf{x})+S_{bc}\ \cos(2\pi\mathbf{k}_{bc}\cdot\mathbf{x}) \\ &+ S_{ca}\ \cos(2\pi\mathbf{k}_{ca}\cdot\mathbf{x}), \end{aligned} \tag{6}$$

where S_{ab}, S_{bc}, S_{ca} are shorthand for $\tilde{S}(\mathbf{k}_{ab})$, $\tilde{S}(\mathbf{k}_{bc})$, $\tilde{S}(\mathbf{k}_{ca})$, with $\tilde{S}(\mathbf{k})$ being the Fourier transform of $S(\mathbf{x})$. Since the function $S(\mathbf{x})$ is normalized according to $\int \mathrm{d}^2\mathbf{x}\, S(\mathbf{x})=1$, it follows that $\tilde{S}(\mathbf{k})\le 1$ for "typical" sources. Hence, each of the interference terms is weighted by a factor less than or equal to unity, i.e., partial interference.

It can be verified that the three-wave interference pattern in Eq. (6) will also be produced, apart from a constant background term, by the following *effective* wave function:

$$\begin{aligned} \psi'(\mathbf{x}) = &\left(\frac{S_{ab}S_{ca}}{S_{bc}}\right)^{1/2} e^{2\pi i\mathbf{k}_a\cdot\mathbf{x}}+\left(\frac{S_{bc}S_{ab}}{S_{ca}}\right)^{1/2} e^{2\pi i\mathbf{k}_b\cdot\mathbf{x}} \\ &+\left(\frac{S_{ca}S_{bc}}{S_{ab}}\right)^{1/2} e^{2\pi i\mathbf{k}_c\cdot\mathbf{x}}. \end{aligned} \tag{7}$$

Hence, in the special case of three-wave interference, an *arbitrary* degree of spatial coherence still permits an interpretation of the intensity, apart from a constant background, in terms of three *coherent* plane waves. In a restricted sense, the introduction of partial coherence can be regarded as producing a change in the amplitudes of the three waves. Importantly for the present work, if the intensity distribution in Eq. (6) is to contain minima that are stable against phase perturbations, then this is equivalent to demanding that the effective wave function ψ' contains *vortices*. Hence, ψ' must vanish at certain points (see Fig. 1), which, it can be shown, requires that the source's Fourier coefficients satisfy the triangle inequalities:

$$\begin{aligned} &S_{ab}S_{ca} < S_{bc}S_{ab}+S_{ca}S_{bc}, \\ &S_{bc}S_{ab} < S_{ca}S_{bc}+S_{ab}S_{ca}, \\ &S_{ca}S_{bc} < S_{ab}S_{ca}+S_{bc}S_{ab}. \end{aligned} \tag{8}$$

These inequalities are summarized graphically in Fig. 6.

For simplicity, the effective source is now assumed to be rotationally-symmetric, corresponding to approximately round Kohler illumination, as used in the experiments described above. For the present setup, where three-wave interference is produced by two biprisms separated by 60°, two of the difference wave vectors, $\mathbf{k}_{ab}$ and $\mathbf{k}_{bc}$, say, are equal in length, while the other, $\mathbf{k}_{ca}$, is longer by a factor of $\sqrt{3}$. Hence, in this case $S_{ab}\approx S_{bc}$ and $S_{ca}=xS_{ab}$, where $0<x<1$. From the triangle inequalities (or Fig. 6), the degree of coherence must satisfy $x>1/2$ in order for ψ' to contain vortices. If the effective source is further assumed to be Gaussian-distributed, then $\tilde{S}(\mathbf{k})=e^{-\mathbf{k}^2/2\sigma^2}$, and the condition for vortices becomes $\mathbf{k}_{ca}^2<2\sigma^2\ln 2+\mathbf{k}_{ab}^2$. For a given source size σ, this places a constraint on the size of the lattice that can contain stable minima. For lattice sizes down to $\sim$1 nm, this requirement can be easily satisfied in a modern FEG-TEM. However, for significantly smaller

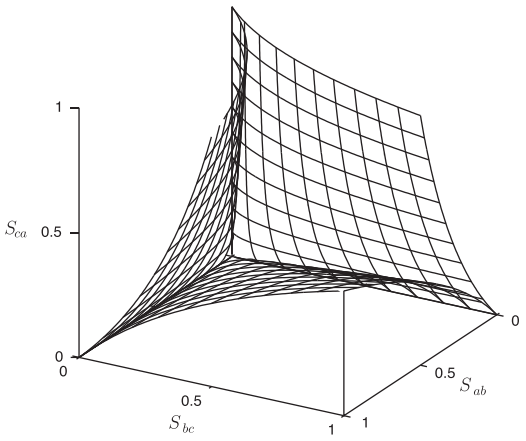

Fig. 6. Spatial coherence requirements for stable three-wave lattices. The effective wave function will contain vortices if the triplet of Fourier coefficients (S_{ab}, S_{bc}, S_{ca}) corresponds to a point that lies between the three curved surfaces. Points that lie exactly on one of the surfaces correspond to effective wave functions in which the vortex–antivortex pairs coincide, i.e., vortex creation or annihilation.

lattices, with a size of about 0.1 nm or less, this requirement may become increasingly difficult to satisfy while maintaining an adequate beam intensity.

7. Conclusion

The generation of three-wave electron vortex lattices using two biprisms was demonstrated. The presence of vortex–antivortex pairs in the lattice was proved unequivocally by using a third biprism to perform a direct phase measurement. Similar measurements could also be used to verify the presence of vortices in irregular arrays of vortices, such as those produced by three interfering spherical waves [14], those contained in electron Airy beams [25], or those contained in electron-optical catastrophes [2].

The accuracy of the vortex positions was discussed, and it was argued that it is more accurate to measure the positions directly from the intensity minima in the three-wave interference pattern, rather than the holographically-retrieved phase. For the case considered, the vortex position accuracy corresponded to a phase accuracy of $2\pi/200$ at a spatial resolution of 1 nm.

An analysis of the coherence requirements for three-wave vortices was presented. It was demonstrated that, even for an arbitrary degree of partial coherence, a three-wave interference pattern can be interpreted in terms of an effective coherent superposition of three plane waves (apart from a constant background). However, if the interference pattern is to contain minima that are stable against phase perturbations, then certain requirements of partial coherence must be met.

Finally, the two-biprism setup demonstrated here should permit nanoscale electromagnetic field measurements via vortex interferometry. Such measurements will form the subject of a future publication.

Acknowledgments

The authors acknowledge the European Commission for an Advanced Grant, and the Deutsche Forschungsgemeinschaft for a Deutsch-Israelische Projektkooperation Grant.

References

[1] J. Verbeeck, H. Tian, P. Schattschneider, Nature 467 (2010) 301.
[2] T.C. Petersen, M. Weyland, D.M. Paganin, T.P. Simula, S.A. Eastwood, M.J. Morgan, Phys. Rev. Lett. 110 (2013) 033901.
[3] L. Clark, A. Béché, G. Guzzinati, A. Lubk, M. Mazilu, R. Van Boxem, J. Verbeeck, Phys. Rev. Lett. 111 (2013) 064801.
[4] J. Masajada, A. Popiolek-Masajada, D.M. Wieliczka, Opt. Commun. 207 (2002) 85.
[5] J. Masajada, Opt. Commun. 239 (2004) 373.
[6] S.A. Eastwood, A.I. Bishop, T.C. Petersen, D.M. Paganin, M.J. Morgan, Opt. Express 20 (2012) 13947.
[7] K.W. Nicholls, J.F. Nye, J. Phys. A: Math. Gen. 20 (1987) 4673.
[8] J. Masajada, B. Dubik, Opt. Commun. 198 (2001) 21.
[9] K. O'Holleran, M.J. Padgett, M.R. Dennis, Opt. Express 14 (2006) 3039.
[10] M.R. Dennis, K. O'Holleran, M.J. Padgett, Prog. Opt. 53 (2009) 293.
[11] J. Becker, P. Rose, M. Boguslawski, C. Denz, Opt. Express 19 (2011) 9848.
[12] P. Kurzynowski, W.A. Wozniak, E. Fraczek, Appl. Opt. 45 (2006) 7898.
[13] S. Vyas, P. Senthilkumaran, Appl. Opt. 46 (2007) 2893.
[14] G. Ruben, D.M. Paganin, Phys. Rev. E 75 (2007) 066613.
[15] J. Masajada, A. Popiolek-Masajada, M. Leniec, Opt. Express 15 (2007) 5196.
[16] L.J. Allen, H.M.L. Faulkner, M.P. Oxley, D.M. Paganin, Ultramicroscopy 88 (2001) 85.
[17] T. Hirayama, T. Tanji, A. Tonomura, Appl. Phys. Lett. 67 (1995) 1185.
[18] K. Miyashita, K. Yamamoto, T. Hirayama, T. Tanji, J. Electron Microsc. 53 (2004) 577.
[19] T. Niermann, J. Verbeeck, M. Lehmann, Ultramicroscopy 136 (2014) 165.
[20] E. Fraczek, W. Fraczek, J. Masajada, Optik 117 (2006) 423.
[21] K. Harada, T. Akashi, Y. Togawa, T. Matsuda, A. Tonomura, J. Electron Microsc. 54 (2005) 19.
[22] T. Niermann, M. Lehmann, Micron 63 (2014) 28.
[23] H. Gavin, The Levenberg–Marquardt method for nonlinear least squares curve-fitting problems, ⟨http://people.duke.edu/~hpgavin/ce281/lm.pdf, 2011 (accessed 15 May 2014).
[24] G. Gbur, T.D. Visser, Prog. Opt. 55 (2010) 285.
[25] N. Voloch-Bloch, Y. Lereah, Y. Lilach, A. Gover, A. Arie, Nature 494 (2013) 331.